Supporting Information for

Narrowing in the differences of urban and non-urban surface ozone levels in summers of the Northern Hemisphere

Han Han[1], Lin Zhang[1,*], Zehui Liu[1], Xu Yue[2], Lei Shu[3], Yuanhang Zhang[4,*]

[1]Laboratory for Climate and Ocean-Atmosphere Studies, Department of Atmospheric and Oceanic Sciences, School of Physics, Peking University, Beijing 100871, China

[2]Jiangsu Key Laboratory of Atmospheric Environment Monitoring and Pollution Control, Collaborative Innovation Center of Atmospheric Environment and Equipment Technology, School of Environmental Science and Engineering, Nanjing University of Information Science & Technology, Nanjing 210044, China

[3]School of Environmental Science and Engineering, Southern University of Science and Technology, Shenzhen 518055, China

[4]State Key Joint Laboratory of Environmental Simulation and Pollution Control, College of Environmental Sciences and Engineering, Peking University, Beijing 100871, China

Correspondence to: Lin Zhang (zhanglg@pku.edu.cn) and Yuanhang Zhang (yhzhang@pku.edu.cn)

Text S1. Ozone data and trend analysis

Surface ozone measurements from TOAR, CNEMC, EPA, and EEA were used in this study. Measurements from TOAR, EPA, and EEA were combined over the TOAR observation sites. TOAR global surface ozone dataset covers the time period of 1970–2015 (Schultz et al., 2017a). Considering the density of the stations, TOAR observations since 1990 were used. Ozone data from EPA and EEA were used to expand the temporal coverage of ozone observations over the TOAR sites in the US and Europe to 2020 by matching the locations of observation sites with TOAR. Ozone dataset from CNEMC covers the time period of 2013–2020. We calculated the MDA8 ozone concentrations over each site at each day in universal time (UTC). We used the European Union definition of the daily 8-hour window starting from 17 UTC of the previous day, and additionally, a MDA8 value is saved only if at least 18 out of the 24 8-hour averages are valid for each day. A monthly mean is saved only when at least 23 days in that month have valid MDA8 values.

We estimated the trend in surface ozone with the linear regression model as the following:

$$y_t = \alpha + \beta t + \gamma \cos\left(\frac{2\pi M}{3}\right) + \delta \sin\left(\frac{2\pi M}{3}\right) + R_t \qquad (S1)$$

where y is the monthly mean ozone concentration, t is a monthly index from January 1990 to December 2020, α is a constant, β is a linear trend, γ and δ are coefficients for a 3-month harmonic series of seasonal cycle (M=1, 2, 3), and $R_t = \rho R_{t-1} + \varepsilon_t$, which accounts for autocorrelation with ε_t representing a normal random error series. Trends estimated by the method are not disproportionately affected by outliers as the time series are comprised of long-term monthly values (Cooper et al., 2020).

Text S2. Population and nighttime light data

For the classification of urban and non-urban ozone observation sites, we used the population density dataset of the Gridded Population of the World, Version 4

(GPWv4) at a horizontal resolution of ~5 km for 2015 accessed from the Socioeconomic Data and Applications Center (SEDAC) at Columbia University (https://sedac.ciesin.columbia.edu/data/set/gpw-v4-population-density-rev11/data-download). The nighttime light dataset was the version 4 Defense Meteorological Satellite Program (DMSP) Operational Linescan System (OLS) product at a horizontal resolution of ~1 km for 2013 downloaded from the National Oceanic and Atmospheric Administration (NOAA) Earth Observation Group (EOG) (https://ngdc.noaa.gov/eog/dmsp/downloadV4composites.html).

Table S1. Classification scheme of urban and non-urban sites.

Station category	Rule	Number of sites
Urban	(1) Population density $\geqslant$ 1000 people km^{-2} (2) Nighttime lights $\geqslant$ 60 (3) Nighttime lights within a 25 km radius of the monitoring site = 63	3302
Suburban	(1) 200 < Population density $\leqslant$ 1000 people km^{-2} (2) Nighttime lights < 60 (3) Nighttime lights within a 5 km radius of the monitoring site > 25	1815
Rural	(1) Population density $\leqslant$ 200 people km^{-2} (2) Nighttime lights within a 5 km radius of the monitoring site $\leqslant$ 25 (3) NO_2 column $\leqslant$ 8×10^{15} molec cm^{-2}	1447
Unclassified	All others	5115

Table S2. Station information of the urban-suburban and urban-rural pairs in regions and cities worldwide. Trends in urban vs. non-urban ozone over Los Angeles are examined using observations over 2001–2015, as the location of the rural observation sites changed in 2001.

	Number of pairs		Number of sites			Period
	Urban-suburban	Urban-rural	Urban	Suburban	Rural	Years
Globe	4152	2209	1568	813	624	
North America	329	441	385	152	341	1990–2020
Europe	1374	1099	307	407	240	1990–2020
East Asia	2444	342	824	245	32	
China	165	9	366	92	5	2013–2020
Korea	200	122	170	9	6	1990–2014
Japan	2079	211	284	143	17	1990–2014
Los Angeles	0	31	14			1990–2015
Montreal	11	76	11			1990–2013
Boston	26	19	6			1990–2020
Madrid	0	76	27			1997–2011
Paris	11	1	9			2001–2012
Zurich	36	17	4			1990–2020
Berlin	56	105	5			1990–2020
Seoul	173	22	86			2001–2014
Tokyo	326	0	19			1990–2013
Sydney	0	21	7			1994–2014
Beijing	7	0	7			2013–2020
Lanzhou	2	1	3			2013–2020
Guangzhou	10	0	11			2013–2020
Hangzhou	7	0	7			2013–2020

Table S3. Trends in air temperature at 2 m (T2m), relative humidity at 2 m (RH2m), and wind speed at 850 hPa (WS850) in cities worldwide over the available observation period in boreal summer.

	T2m (°C per decade)			RH2m (% per decade)			WS850 (m/s per decade)		
	Urban	Suburban	Rural	Urban	Suburban	Rural	Urban	Suburban	Rural
Los Angeles	0.6		0.7	−5.4		−7.3	0.0		−0.0
Montreal	0.1	0.4	0.2	1.1	0.5	1.5	−0.3	−0.7	−0.3
Boston	0.4	0.2	0.6	0.2	1.6	−2.3	−0.2	−0.1	−0.2
Madrid	0.2		−0.7	−3.1		−2.6	−0.0		−0.3
Paris	−0.7	−0.7	−1.1	−2.5	−3.3	−1.0	1.2	1.1	1.6
Zurich	0.1	0.2	1.1	0.5	−0.3	−1.3	−0.1	−0.1	0.2
Berlin	0.6	0.6	0.5	−1.3	−1.4	−0.8	−0.3	−0.3	−0.3
Seoul	1.0	2.0	0.7	1.2	−3.4	0.7	−0.3	−0.3	−0.3
Tokyo	0.4	0.4		−0.3	−0.6		0.3	0.4	
Sydney	−0.1		0.0	0.7		0.8	0.4		0.4
Beijing	0.4	1.2		3.8	−0.7		0.2	0.3	
Lanzhou	−0.6	−0.9	−1.6	4.7	4.1	21.8	1.3	0.6	−0.8
Guangzhou	0.5	0.5		4.5	4.6		0.4	0.5	
Hangzhou	−0.2	−0.3		12.5	13.0		0.6	0.7	

Table S4. Mean urban vs. suburban and urban vs. rural MDA8 ozone differences (in ppbv) in cities worldwide over the available observation period in boreal summer in each decade.

	Urban−suburban			Urban−rural		
	1990s	2000s	2010s	1990s	2000s	2010s
Los Angeles					−11.8	−5.7
Montreal				−9.5	−4.2	−2.3
Boston	−4.1	−2.6	−2.2	−10.8	−6.0	−2.3
Madrid				−17.5	−12.4	−3.3
Paris		−1.8	−2.7		−2.2	0.4
Zurich	−7.6	−4.8	−4.5	−18.3	−12.1	−9.8
Berlin	−13.1	−7.1	−1.3	−11.0	−8.4	0.3
Seoul		−3.8	−4.1		0.9	−1.9
Tokyo	−8.8	−2.6	−0.5			
Sydney				−7.2	−7.3	−5.4
Beijing			3.5			
Lanzhou			4.2			−7.4
Guangzhou			1.4			
Hangzhou			5.1			

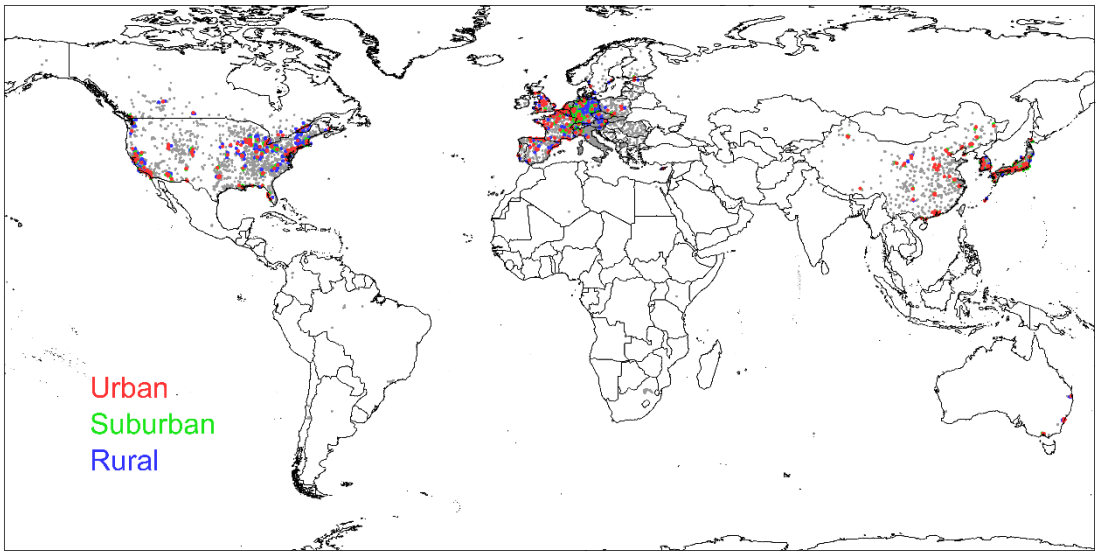

Figure S1. Paired urban (in red), suburban (in green), and rural (in blue) ozone observation sites over the globe. The grey dots indicate the observation sites that are not used in the examination of urban vs. non-urban ozone differences in this study.

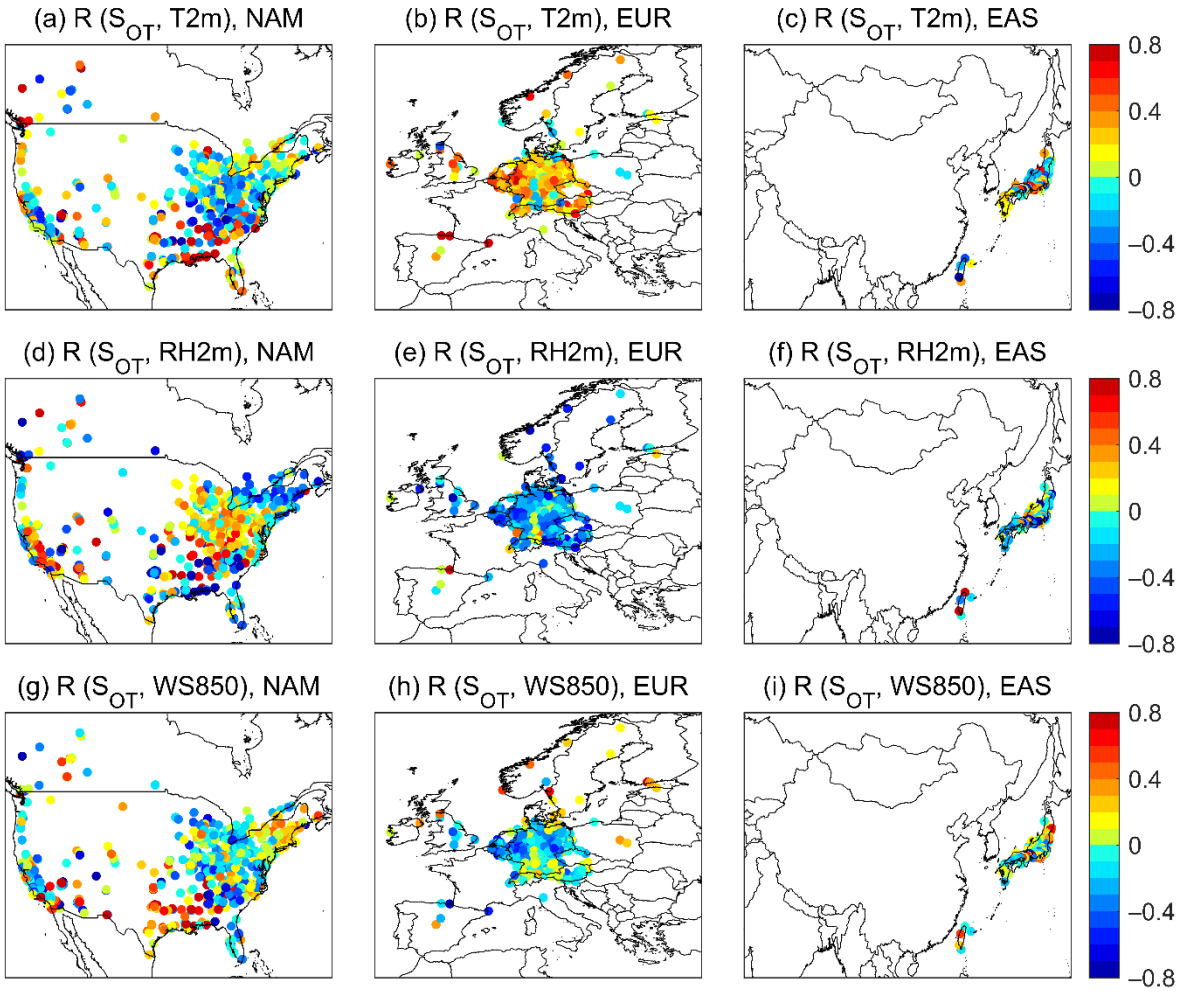

Figure S2. Correlation coefficients (R) between the surface MDA8 ozone vs. 2-m temperature (T2m) regression slope (S_{OT}) and 2-m temperature (a–c), 2-m relative humidity (RH2m) (d–f), and wind speed at 850 hPa (WS850) (g–i) in North America (NAM), Europe (EUR), and East Asia (EAS) in summer. The observations with over 15-year continuous records are used in the calculation.

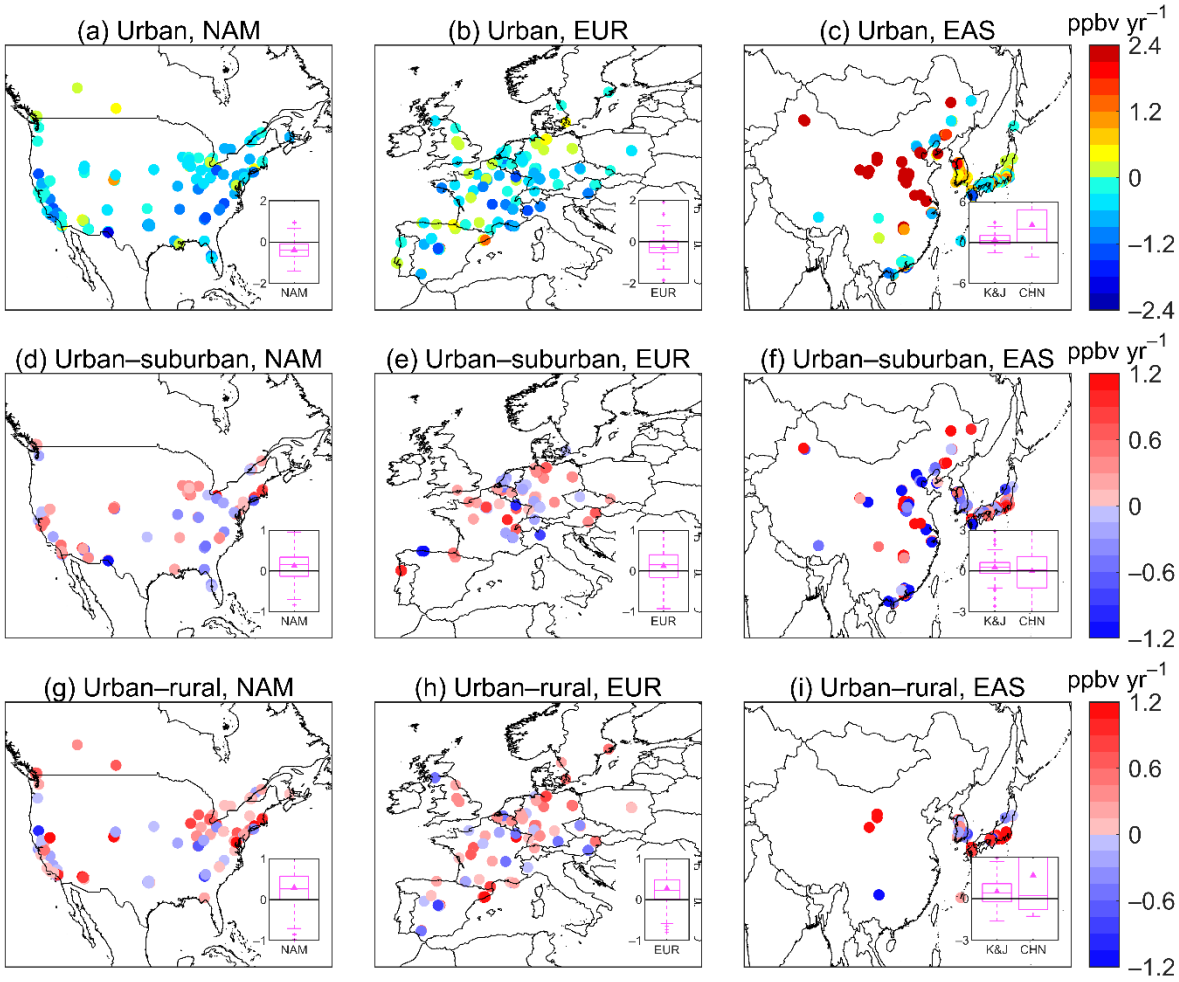

Figure S3. Trends in urban MDA8 ozone concentrations (a–c), urban vs. suburban MDA8 ozone differences (d–f), and urban vs. rural MDA8 ozone differences (g–i) in boreal summer in North America (NAM), Europe (EUR), and East Asia (EAS). Values are calculated over 2000–2014 in North America, Europe, and Korea and Japan (K&J), and over 2013–2020 in China (CHN). Box-whisker plots (25th percentile, median, 75th percentile, and lines above/below the box denote 95th/5th percentiles) with triangles indicating the regional means are shown inset.

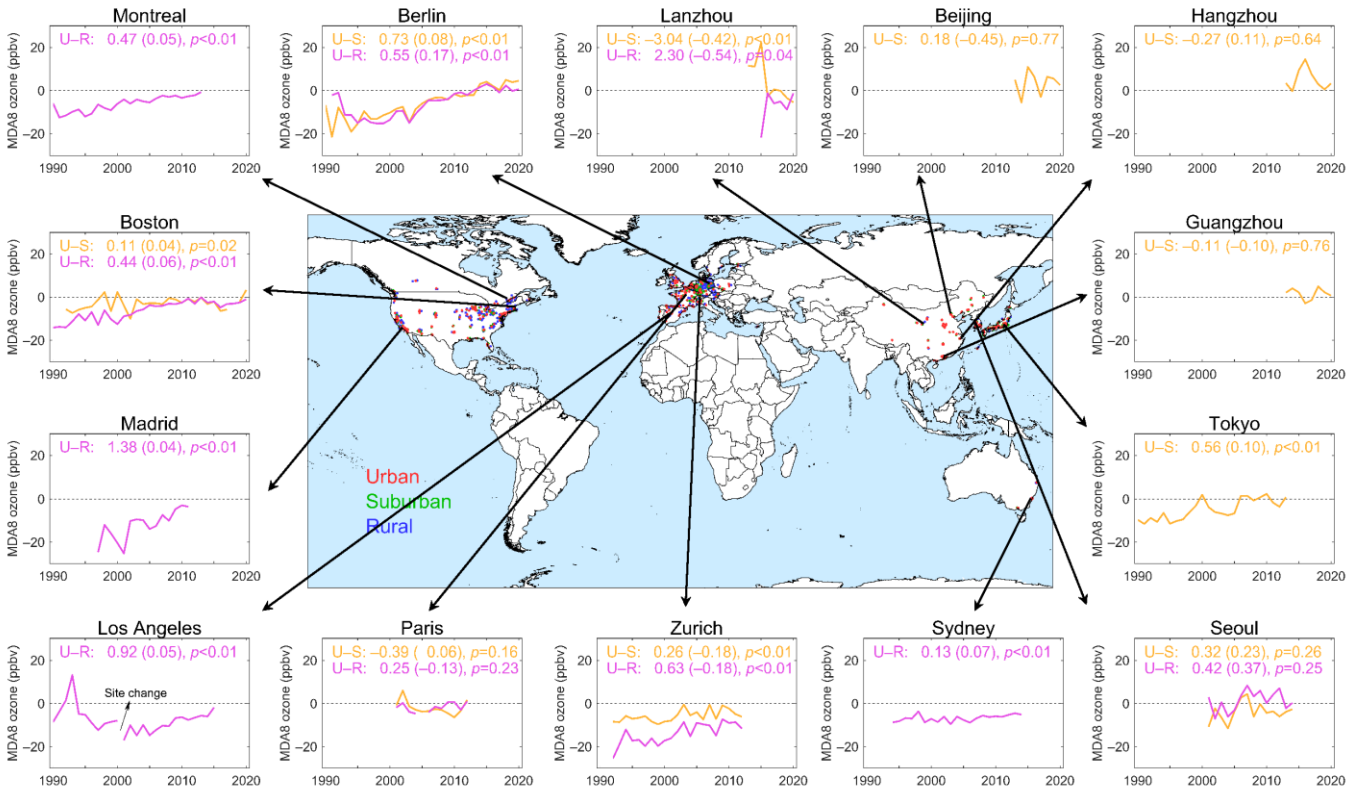

105 **Figure S4**. Trends (ppbv yr^{-1}) in urban vs. suburban (U−S, in brown) and urban vs. rural (U−R, in purple) ozone differences over cities worldwide in boreal summer. The central panel shows the global distribution of paired sites. The number of sites and available observation period are shown in Table S2. Numbers in the brackets show the contributions of changes in climate to the trends in urban vs. non-urban ozone

110 differences as estimated by the GMLR model.

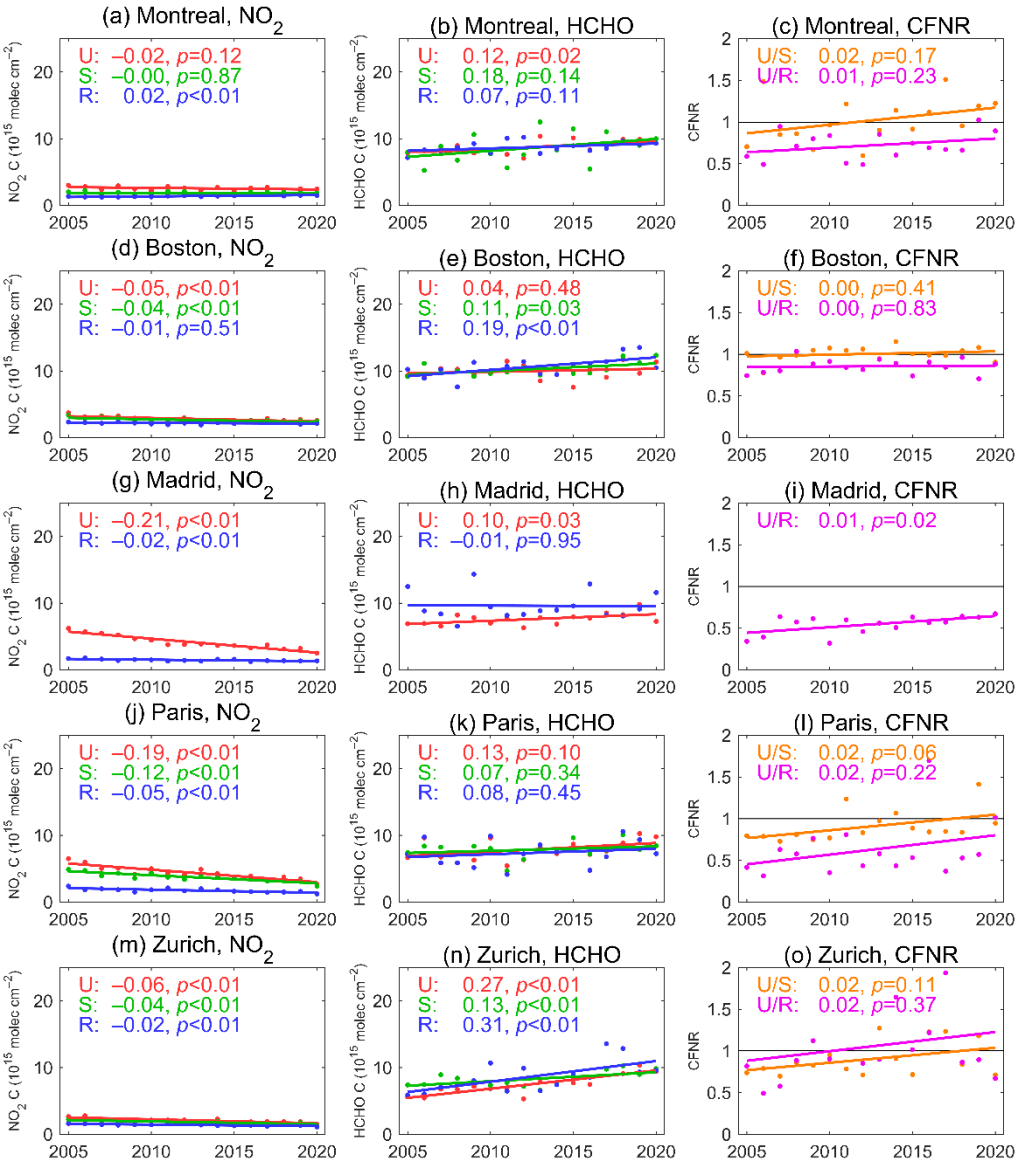

Figure S5. Trends in OMI observed boreal summer mean NO_2 tropospheric columns (left panels), HCHO columns (middle panels), and urban vs. non-urban contrasts of HCHO/NO_2 ratios (CFNR, right panels; also see Section 3.2 in the main text) in five cities (Montreal, Boston, Madrid, Paris, Zurich) from 2005 to 2020. Linear regression lines are shown for urban (U) values in red, suburban (S) values in green, and rural (R) values in green, urban vs. suburban (U/S) CFNR in orange, and urban vs. rural (U/R) CFNR in purple. The linear regression slopes and *p* values are shown inset. CFNR values of close to 1 indicate similar ozone formation regimes between urban and non-urban areas.

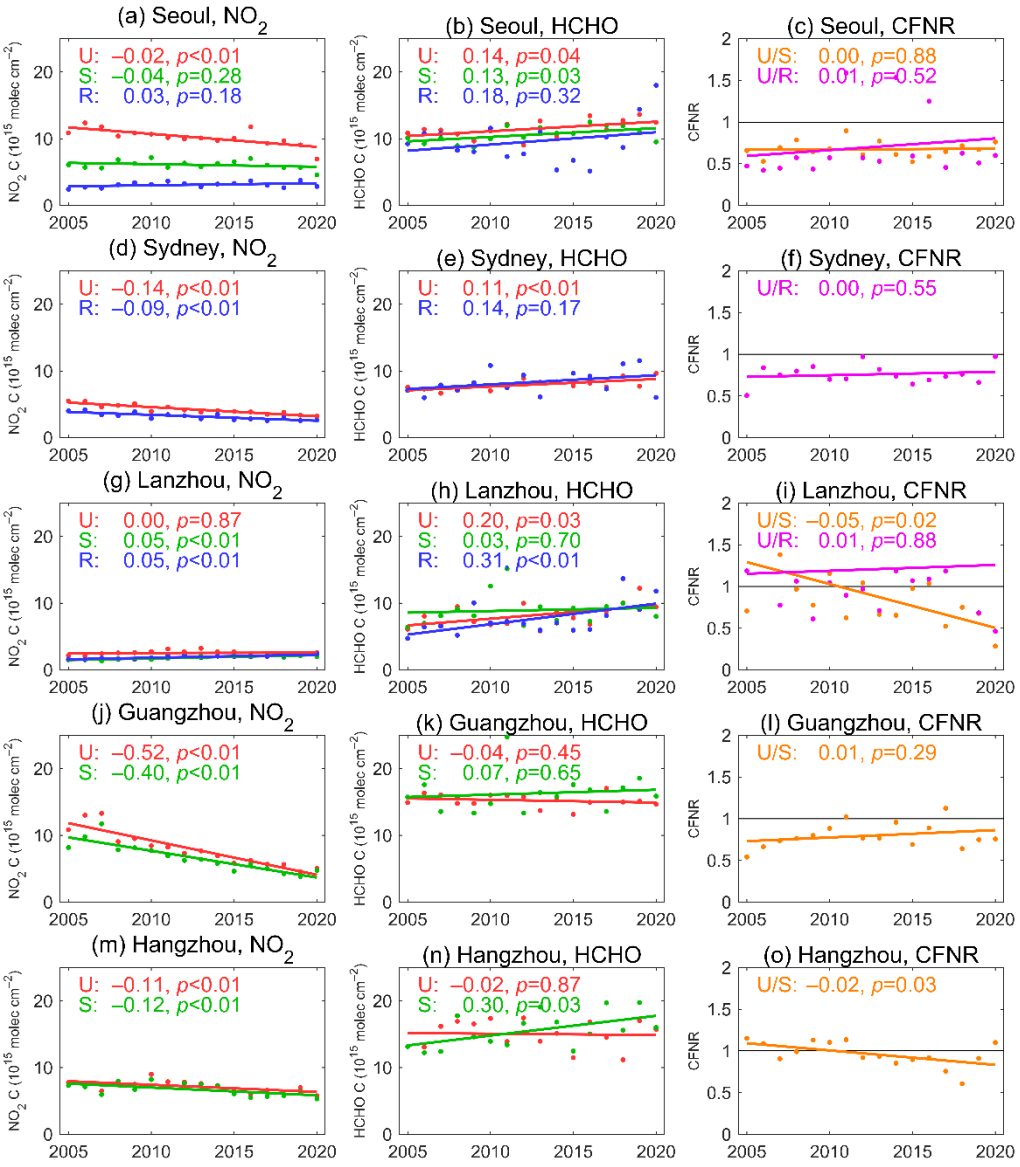

Figure S6. The same as Figure S5, but for cities: Seoul, Sydney, Lanzhou, Guangzhou, and Hangzhou.

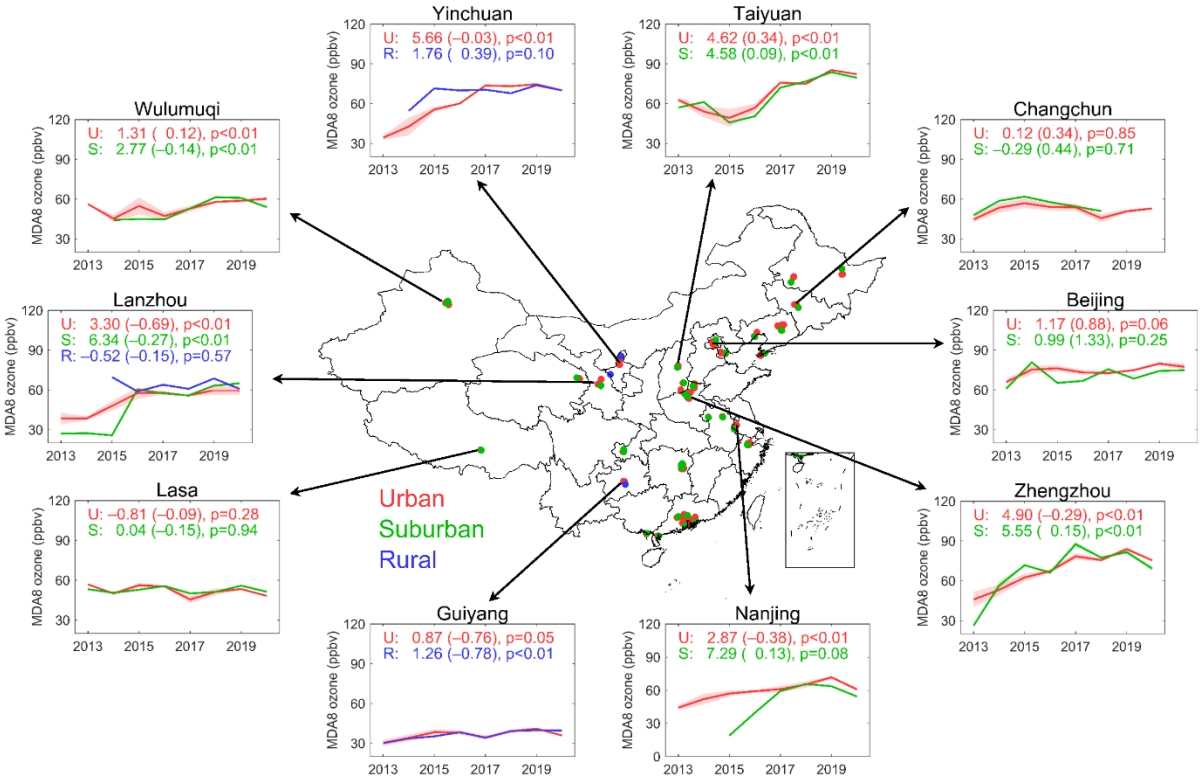

Figure S7. Comparison of surface MDA8 ozone concentrations and trends (ppbv yr^{-1}) over urban (U, in red), suburban (S, in green), and rural (R, in blue) areas in summer in China during 2013–2020. The central panel shows the spatial distribution of paired sites. Numbers in the brackets show the contributions of changes in meteorology to the ozone trends as estimated by the GMLR model.